Local strain fields in paper

M. J. KORTEOJA, A. LUKKARINEN, K. KASKI, D. E. GUNDERSON, J. L. DAHLKE, AND K. J. NISKANEN

ABSTRACT

When a paper specimen is strained microscopic ruptures give rise to plastic deformations. These deformations can be made visible by silicone impregnation. We show that the plastic deformations or strains are nonuniform on the microscopic and macroscopic scale. Large fractions of a typical paper specimen do not enter the plastic region before rupture, even though the macroscopic behavior may be highly plastic. Computer simulations are employed to evaluate the macroscopic strain variations and the changes in paper properties that are induced by formation-type disorder. We show that increasing disorder reduces the number of plastic yield sites.

THE FORMATION, OR LARGE-scale uniformity, of paper affects its mechanical behavior *(1)* and particularly tensile strength. When a paper specimen is stretched, light-weight areas generally elongate more than heavy-weight areas. Local strains vary usually as much as the basis weight varies, but sometimes clearly more *(2–4)*.

Even though formation has an obvious effect on the mechanical properties of paper, no precise one-to-one relationship exists between the local basis weight and strain fields in any given paper specimen. There are two reasons for this. First, variation in basis weight does not in itself account for variations in network structure. The degree of bonding, fiber density, fines and filler content, and drying strains all play a significant role. Second, local deformations depend also on the surrounding basis weight values and, therefore, must be correlated over short distances. In this paper we focus on the latter, topological aspects of local deformations.

Short-range spatial correlations of local strains have in the past been illustrated in a few cases using the finite element method *(3–5)* or direct observations *(2, 6, 7)*. It has been shown that lightweight areas in paper can be reinforced or "shielded" by adjacent heavier areas *(3, 5)*. Also, the average strain in any given transverse section of a paper specimen is inversely proportional to the average basis weight of that section. Along such a section, in the transverse direction, strain varies more smoothly than the basis weight *(4)*. Moffatt *et al. (8)* have shown that the breaking zone in newspaper strips had consistently lower basis weights than the average basis weight for the specimen as a whole. An interesting observation of the spatial strain correlations was first made by Rance *(9)* and later discussed in detail by Ranger and Hopkins *(6)*. They found that plastic (irreversible) deformations in paper seem to concentrate along lines that traverse across the specimen at a 30°–40° angle to the external stress.

In this paper, we study the localization of plastic strain and ultimate failure on the length scale of fiber flocs using experiments and computer simulations *(10)*. The statistical effects of the formation-like randomness in paper structure are emphasized. In the simulations, randomness in local elastic modulus is taken to represent the combined effects of local basis weight, fiber orientation, drying strains, and bonding degree. Experiments are used to illustrate the phenomena with real paper.

EXPERIMENT

Specimen papers were a virgin pine kraft, 205 g/m^2 linerboard, and a commercial 47 g/m^2 newsprint. They were saturated with a two-part liquid silicone which cures to a low-modulus, optically clear gel. The gel fills voids within the web structure and thus reduces the incidence of local discontinuities in the index of refraction through the thickness of the paper. The treated paper is significantly more translucent than the original—as would be a wax or oil-filled paper. The treatment causes small but observable increases in tensile modulus and strain to failure.

When the treated specimen is strained in tension small "lines," and then patterns of lines, begin to become apparent with the onset of nonlinearity in the measured stress-strain curves. If the specimen is lit from behind the surface being viewed, the lines appear dark, as in Figs. 1A and 1B. If the specimen is front-lit, the same lines appear white, as in Figs. 1C and 1D.

In machine direction specimens, few—if any—lines are observed at any level of strain up to failure. In cross machine direction (CD) specimens, the lines begin to become apparent at less than half the failing strain, become profuse as strain increases toward failure, and eventually form distinct diagonal patterns. The lines observed in the treated materials are not evident at all in untreated specimens of the same paper. The patterns we have observed tend to be concentrated around fibers oriented transverse to the direction of applied stress. They are "sharp" in the newsprint specimens and "fuzzy" in the heavier

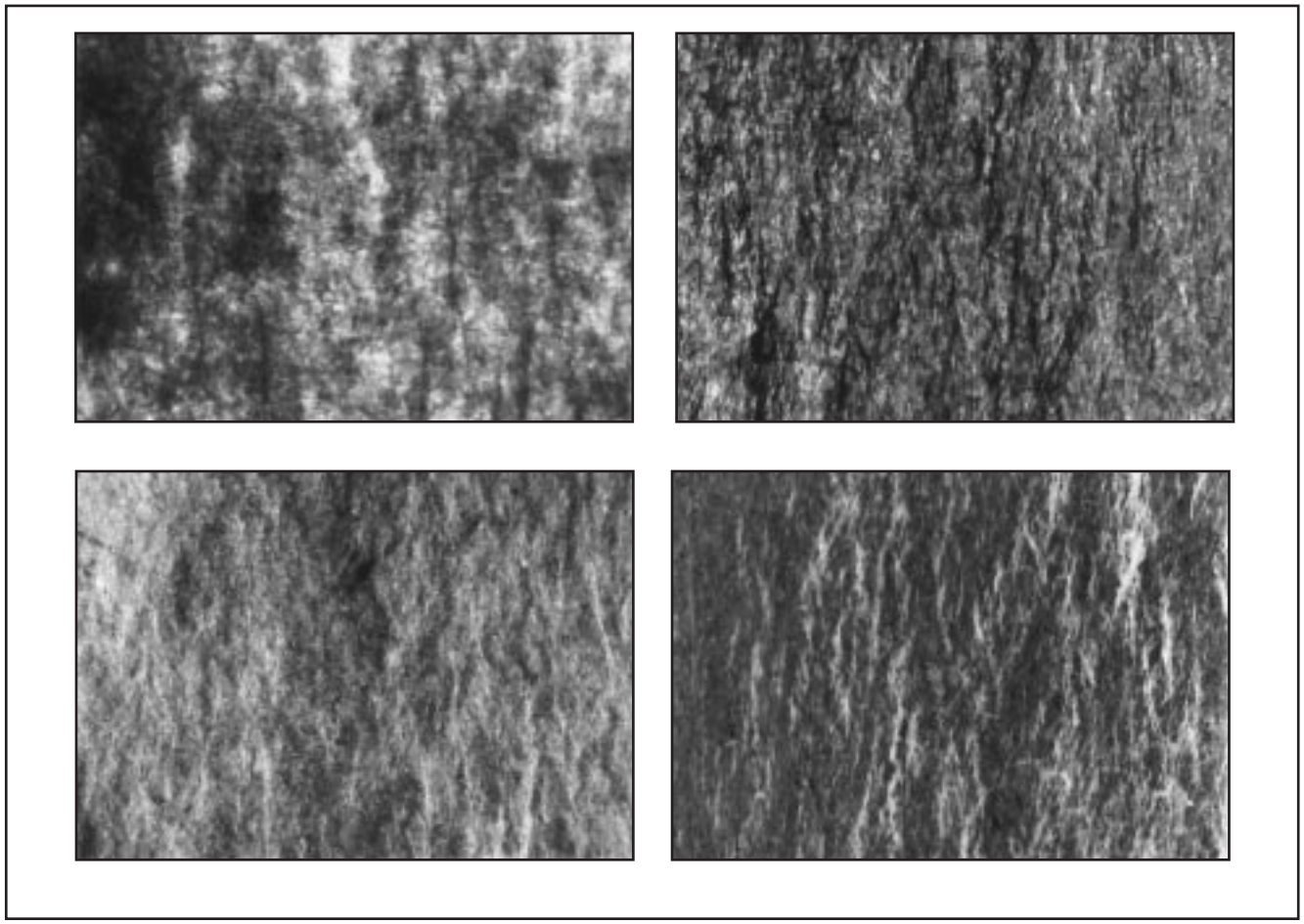

1. Photographs of strained CD paper strips; back-lit linerboard (A) and newsprint (B) at a high magnification (100X), and the same specimens front lit (C and D). Direction of straining is horizontal.

linerboard specimen. The patterns are essentially permanent.

We reason that the lines are evidence of micro-failures within the web structure. The micro-failure creates a discontinuity in the index of refraction within the specimen and therefore is seen light or dark depending on the lighting arrangement. It is well known that the average light-scattering coefficient of paper increases in linear proportion to plastic strain. In both materials, the site of eventual failure can often be visually related to a specific fiber or fiber group long before failure actually occurs.

When viewed with the naked eye, the silicone-treated and strained specimens display nonuniform "criss-cross" patterns (Fig. 2). Sometimes nearly-diagonal strain lines are apparent. Similar lines have been observed earlier by Rance *(9)* and by Ranger and Hopkins *(6)* in tracing paper which by its translucent nature is optically quite similar with the silicone-treated paper used here. Rance had already concluded indirectly that similar patterns must occur in other paper grades as well. Ranger and Hopkins *(6)* also measured local strains directly in a few cases and found that regions of large strain coincided with the lines of increased opacity.

The nonuniform patterns of internal fracture show where the sample elongates plastically. From the photographs, one can see that the spatial distribution of plastic strains in paper is highly nonuniform at the microscopic and macroscopic level. It is also of interest that even though failures at the fiber level appear to concentrate around laterally oriented fibers, the macroscopic strain lines propagate in diagonal directions.

COMPUTER SIMULATIONS

In the computer simulations *(10)*, the specimen is divided into imaginary cells that form a square lattice. The choice of the cell size is arbitrary. Each cell is given an elastic modulus which is to represent the

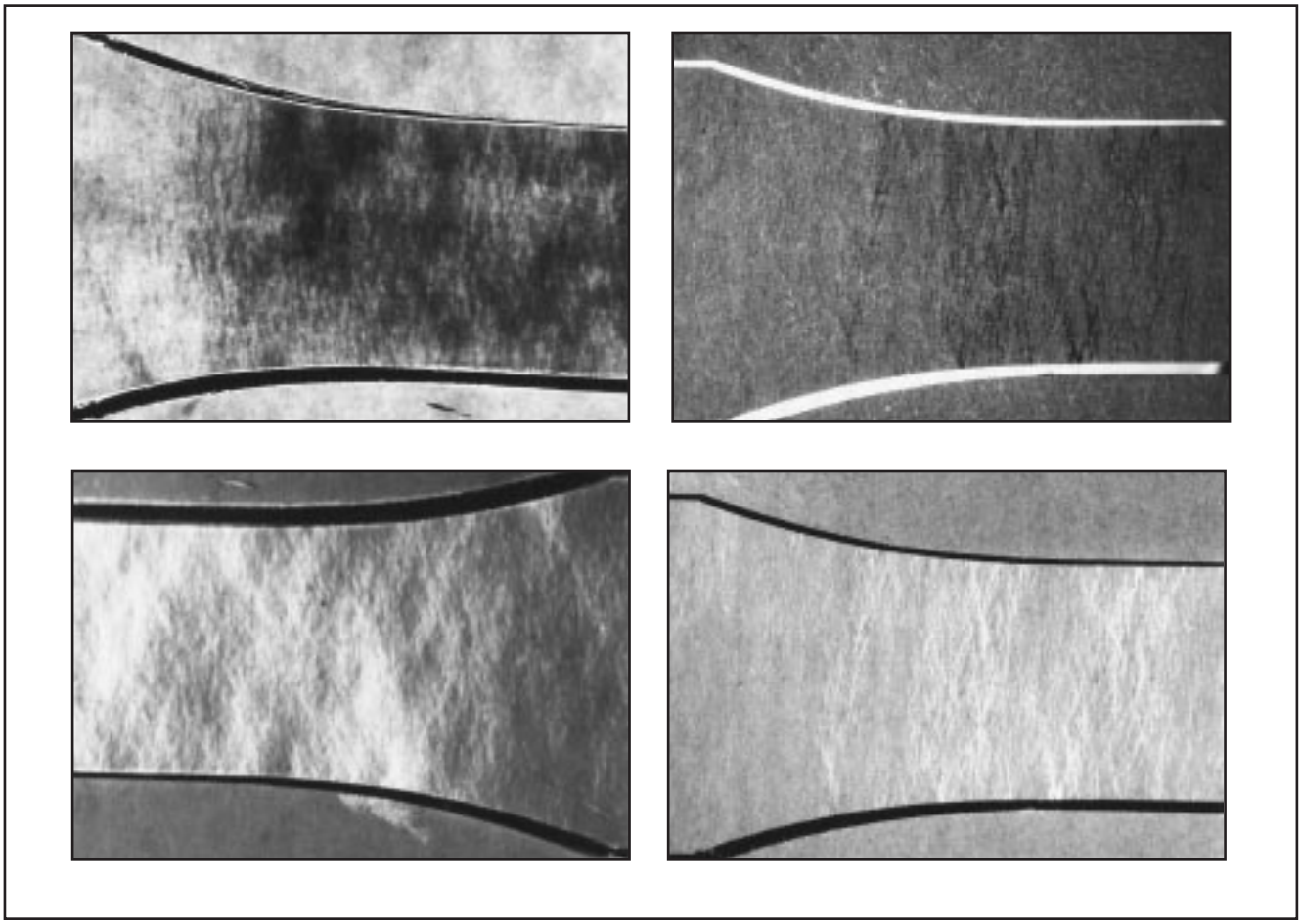

2. Photographs of strained CD paper strips; back-lit linerboard (A) and newsprint (B) at a low magnification, and the same specimens front lit (C and D)

combined effects of randomness in local basis weight, fiber orientation, drying strains, and bonding degree. The elastic modulus is the only source of nonuniformity in the model. The modulus values can be taken, for example, to be proportional to measured local basis weight of real paper (cf. Fig. 4) or they can be randomly assigned as will be explained in the following sections.

The cell corners (nodes of the square lattice) are allowed to move only parallel to the direction of external strain. The uniaxial translation of cell corners leads to three basic deformations (cf. Fig. 3); all other deformations are linear combinations of these three. The deformation of each cell, in response to a given external elongation, is determined by minimizing the total elastic energy of the system (cf. Appendix). If a deformation component exceeds a set limit, then the cell either fails or becomes plastic—depending on the choice of parameters.

There are four factors that define the model system: (1) specimen geometry (in units of the number of cells), (2) the statistical distribution of local moduli (paper "formation"), (3) the ratio *G/E* of the specific shear modulus *G* to the specific Youngs' modulus *E*, and (4) the ratio q_{fr}/q_{pl} of the critical strain for the rupture to that for the plastic yielding. The values specified for Young's modulus and yield strain merely set the scale for stress and strain. The ratios *G/E* and q_{fr}/q_{pl} are material parameters of the model that are taken to be constants. Local shear modulus is assumed to vary in the same way as the local Young's modulus.

In order to illustrate the model performance, we used the measured basis weight distribution of a tissue paper. Local modulus was taken to be proportional to the local basis weight with a scale factor such that the coefficient of variation of the modulus was equal to *CV(E)* = 10%. As Fig. 4 shows, the simulated plastic strain distribution has the same appearance as seen in the experi-

ments (Fig. 2). Hence the model seems to give a fair representation of the behavior of real papers.

In our simulations, we have found that the spatial distribution of local deformations is quite sensitive to the manner in which the local modulus varies. For example, if the modulus variations correspond to randomly assigned flocs, then the shape and size of the flocs and their spatial arrangement can significantly affect the sharpness of the plastic strain lines. Furthermore, the direction of the strain lines depends also on the relative shear stiffness *G/E*. A large *G/E*-value favors lines in the transverse direction while a small value favors strain lines that are parallel to the direction of the external strain. In discussing the strain lines in paper, Ranger and Hopkins *(6)* proposed that the lines must be related to the fibrous structure of paper, more precisely to fiber buckling. However, this cannot be true as we observe the same close-to-diagonal lines in the model where no assumptions are made about the microscopic structure or deformation process. Instead we propose that the spatial distribution of plastic strains is controlled by two factors, the local moduli and the overall elastic properties of paper. Detailed discussion is deferred to another publication.

SIMULATED LOAD-ELONGATION BEHAVIOR

Next we consider the macroscopic load-elongation behavior of paper when the local elastic moduli are in a one-to-one relationship to a random floc structure. The structure is generated by dropping circular flocs of diameter 10 cells randomly on a 30 by 120 cell lattice. The average number of flocs per cell (equal to the basis weight) determines the variability of the local elastic modulus, *CV(E)*. This should give a reasonable approximation to the structure of real paper *(11)*. If flocs in real paper were 5 mm in diameter, then model would mimic the tensile test of a 15-mm wide and 60-mm long paper strip.

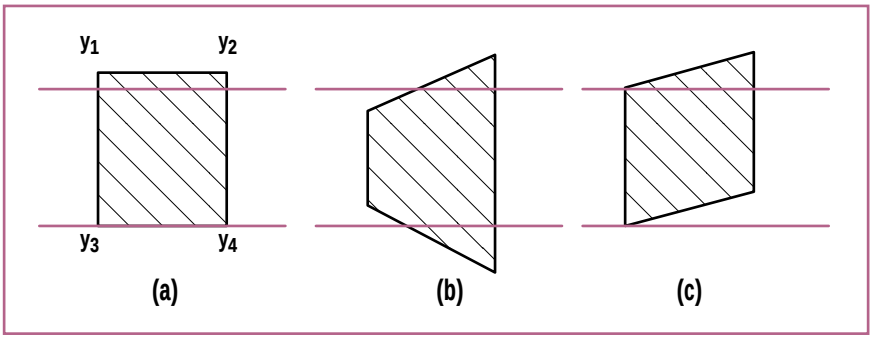

3. The deformation modes of the model cells. The three terms in the elastic energy (cf. Appendix) with prefactors A, B, and C correspond to (a), (b), and (c), respectively.

The thick lines in Fig. 5 present the simulated stress against strain when the model paper is assumed to yield indefinitely without rupture ($q_{fr} = \infty$). The yield threshold is set to $q_{pl} = 5\%$. The thin lines give the fraction of cells, N_{pl}/N_{tot}, that have become plastic at any given external strain. A finite fracture threshold q_{fr} gives otherwise the same behavior but with paper failing at a finite strain. The failure point is indicated in Fig. 5 for $q_{fr}/q_{pl} = 10$ and 100. One can see that, even when the fracture threshold is somewhat larger than the yield threshold, $q_{fr} \leq 10 \times q_{pl}$, the simulated paper still fails at about the macroscopic yield point. The stress and relative number of plastic sites N_{pl}/N_{tot} at the failure point are both sensitive to the ratio q_{fr}/q_{pl}. The behavior with $q_{fr}/q_{pl} = 10$ should apply to real paper when tested in machine direction (MD). In contrast, when the model paper is ductile, the breaking stress and the corresponding value of N_{pl}/N_{tot} increase only very slowly with growing $q_{fr}/q_{pl} \gg 1$. This should be similar to real paper in CD, except that since ideal plasticity does not apply, the breaking stress presumably still increases with increasing q_{fr}/q_{pl}.

Independent of the value of q_{fr}/q_{pl}, the results in Fig. 5 show that N_{pl}/N_{tot} decreases when *CV(E)* increases. In other words, when disorder in modulus increases, a smaller and smaller fraction of the paper area becomes plastic before failure. In a nonuniform paper, plastic deformations start developing at smaller strains and at a slower rate than in a uniform paper. In all cases that we simulated, less than a quarter of the paper area becomes plastic before failure, which is in good agreement with the experiments (cf. Fig. 1).

Finally, we study how the macroscopic elastic modulus of paper depends on the variability of local modulus. To expedite the treatment, we assigned the local modulus values completely at random thus excluding floc-like spatial correlations. The cells can then be considered as having the same size as the average flocs in paper. The local moduli were taken from a uniform distribution. The width of the distribution is proportional to the coefficient variation *CV(E)*. The decrease of the macroscopic elastic modulus against *CV(E)* is shown in Fig. 6 for three different specimen shapes, a narrow strip, a square, and a short specimen. The first one is modeled as a single column of cells and the third with two rows (notice that with a single row of cells the macroscopic modulus would be independent of *CV(E)*). In simulation trials, it

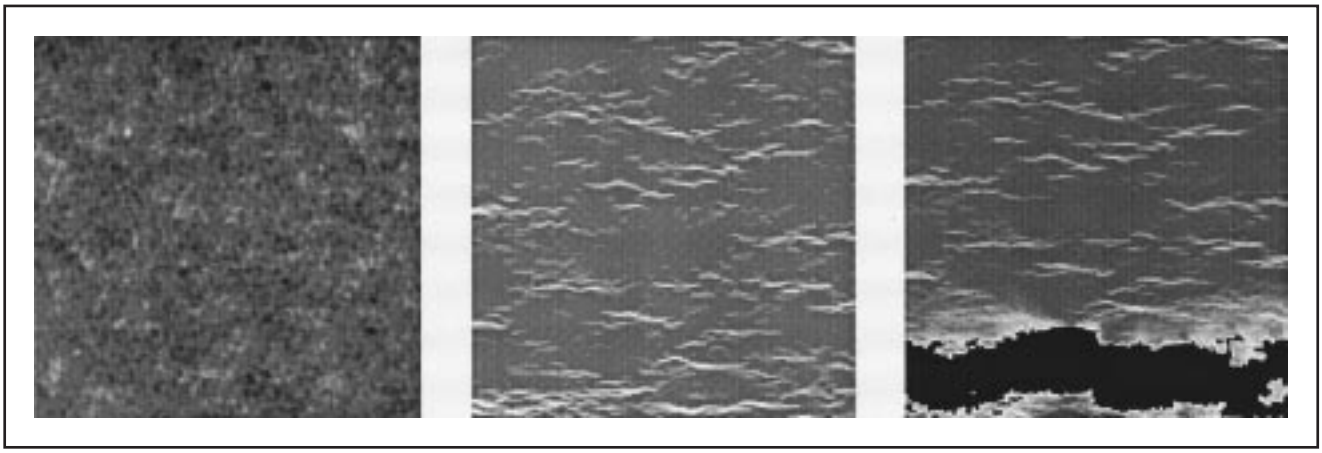

4. Simulated distribution of plastic strains (B) and (C) corresponding to a measured ß-radiogram of tissue paper (A). Low basis weight is shown dark in (A) and plastic deformations are white in (B) and (C) in the same way as in Fig. 2. The 7 x 7-cm² radiogram is represented by 170 x 170 cells in the model.

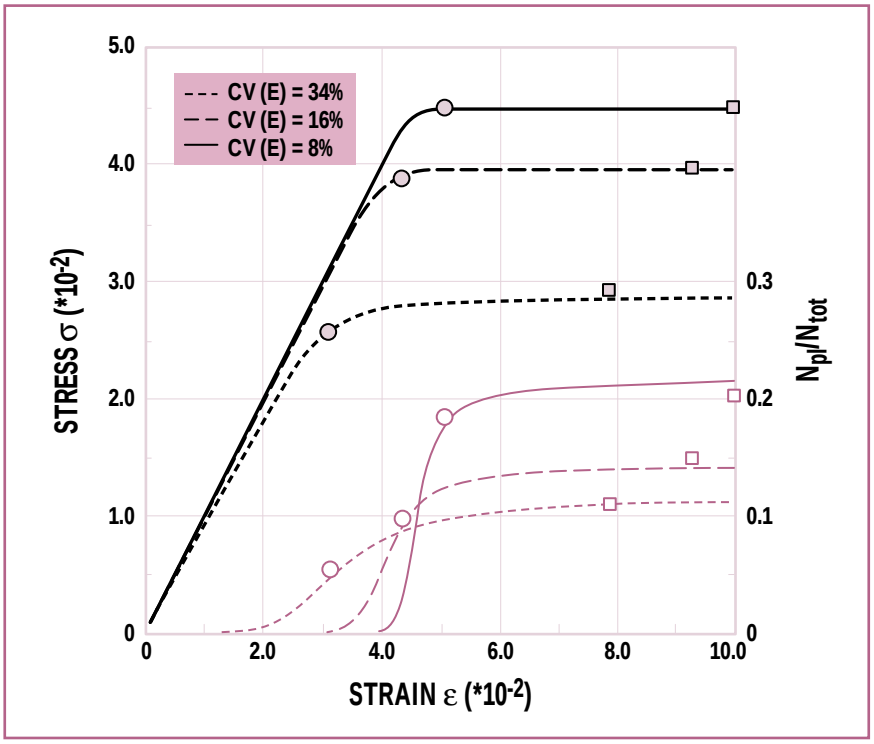

5. Simulated stress (thick lines) and concentration of plastic sites N_{pl}/N_{tot} (thin lines) against external strain for a model of 30 x 120 cells. Flocculated structure with CV(E) = 10%, 20% and 30% (solid line, long dashes and short dashes, respectively). Circles indicate breaking points when q_{fr}/q_{pl} = 10 and squares when q_{fr}/q_{pl} = 100. G/E = 1/4 and q_{pl} = 5%.

turned out that all specimen shapes, except the extreme cases of a very narrow or a very short specimen, gave results that are close to those shown in Fig. 6 for the square specimen. Hence the shape of the tensile strip used in experiments should not have an effect on the formation-dependence of the elastic modulus of real paper. The effect of disorder on the macroscopic modulus is quite weak. Even an unreasonably high value of $CV(E)$ = 30% leads to just a 5% reduction in the macroscopic modulus. The results in Fig. 6 can be approximated by $E = 1 - CV(E)^2/2$ for most specimen shapes. For the one-dimensional single column, the result is $E = 1 - CV(E)^2$, in agreement with an analytic result derived by Dodson *(12)*.

SUMMARY

Highly nonuniform patterns of irreversible internal fracture or plastic strain were observed in strained paper specimens that were treated with silicone. At the microscopic level, the failures seem to concentrate around laterally oriented fibers while, at the macroscopic level, they lie along roughly diagonal lines. The patterns are influenced by the structure and formation of paper being descriptive of the way in which load is carried through the specimen. The patterns often indicate the location of eventual macroscopic failure while the load is well below the maximum value.

The effects of macroscopic formation-type disorder were studied

KEYWORDS
Computer programs, elastic strength, flocs, formation, mechanical properties, paper grades, paper properties, plastic deformation, simulation, strains.

using a computer simulation model where disorder is implemented in the local elastic modulus. When the local modulus was taken proportional to the measured basis weight map of real paper, the simulations gave similar plastic strain patterns as those observed in the experiments. The simulations predict that in all paper grades plastic deformations take place in less than a quarter of the paper area. Increased disorder reduces this fraction. Increased disorder, "poorer formation," also lowers the breaking strength of the model paper, particularly when the breaking threshold strain is close to the yield strain. This would be the case in real paper in MD. TJ

Korteoja, Lukkarinen, and Kaski are, respectively, graduate students and professor, Tampere University of Technology, Tampere, Finland. Gunderson and Dahlke are, respectively, research engineer (retired) and general engineer, USDA Forest Products Laboratory, Madison, WI. Niskanen is senior scientist, KCL Paper Science Centre, Finland (permanent address) and USDA Forest Products Laboratory, Madison, WI.

This study has been partly supported by the Finnish Technology Development Centre (TEKES) and the Academy of Finland, which are gratefully acknowledged.

Received for review June 15, 1995.

Accepted Oct. 31, 1995.

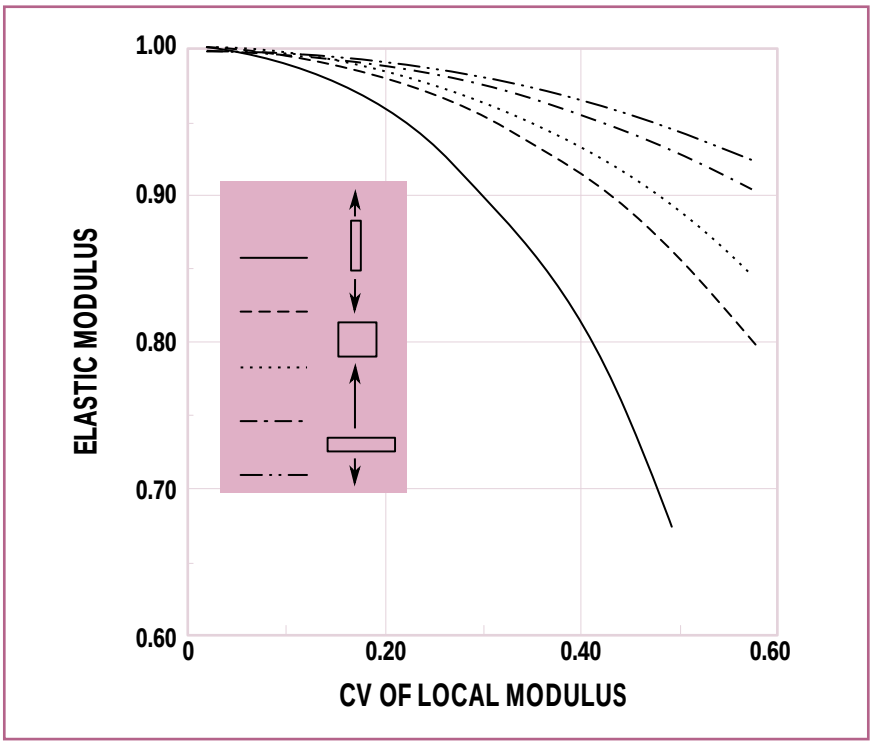

6. Simulated macroscopic elastic modulus E against the coefficient of variation of local modulus CV(E) for a narrow strip (40,000 x 1 cells), square specimen (200 x 200 cells) and short specimen (2 x 20,000 cells), dotted, dashed and dash-dotted line, respectively. G/E = 1 and 1/4 (thin and bold lines, respectively).

LITERATURE CITED

1. Norman, B. and Wahren, D., in *The Fundamental Properties of Paper Related to its Uses* (F. Bolam, Ed.), British Paper and Board Ind. Fed., London, 1976 p. 7.
2. Lyne, M. B. and Hazell, R., in *The Fundamental Properties of Paper Related to its Uses* (F. Bolam, Ed.), British Paper and Board Ind. Fed., London, 1976, p. 74.
3. Thorpe, J. L., *Tappi* 64(7): 119(1981).
4. Kimura, M. and Shimizu, H., *Japan Tappi* 39(9): 859(1985).
5. Kimura, M. and Shimizu, H., *Japan Tappi* 39(8): 777(1985).
6. Ranger, A. E. and Hopkins, L. F., in *Formation and Structure of Paper* (F. Bolam, Ed.), British Paper and Board Makers Assoc., London, 1962, p. 277.
7. Chaves de Oliviera, R., "Stress-strain behavior of low-grammage and/or lightly bonded papers by dot matrix technique," Ph.D. thesis, College of Environmental Science and Forestry, SUNY, Syracuse, 1993.
8. Moffatt, J. M., Beath, L. R., and Mihelich, W. G., in *The Fundamental Properties of Paper Related to its Uses* (F. Bolam, Ed.), British Paper and Board Ind. Fed., London , 1976, p. 104.
9. Rance, H. F., in *Some Recent Developments in Rheology* (V.G.W. Harrison, Ed.), United Trade Press, London, 1950, p. 90.
10. Korteoja, M. J., Lukkarinen, A., Kaski, K., *et al., Phys. Rev.* E51: 1055–1058(1995).
11. Wong, L., Chan, K., Kortschot, M. K., *et al.*, poster P.10 in 1994 International Progress in Paper Physics Seminar, Atlanta, 1994 (unpublished).
12. Dodson, C.T.J., *Handbook of Paper Science* (H. F. Rance, Ed.), Elsevier, Amsterdam, 1982, p 86; Deng, M. and Dodson, C.T.J., *Paper—An Engineered Stochastic Structure*, TAPPI PRESS, Atlanta, 1994, p. 193.

APPENDIX

Details of the simulation model

In the simulations, paper is modeled as a "coarse grained" disordered continuum material, whose microscopic structure is averaged out—local elastic modulus is the only source of disorder. The specimen is divided into a rectangular lattice of adjoined square cells, each defined by the four corner nodes. The elastic energy of the system is written in terms of the longitudinal displacements y_1, y_2, y_3, and y_4 of the corners (cf. Fig. 3) in the following manner:

$$H = \sum_{i=1}^{n} \alpha_i \rho_i \{ A \left(+y_1 + y_2 - y_3 - y_4 - \pi_{A_i} \right)^2 + B \left(-y_1 + y_2 + y_3 - y_4 + \pi_{B1_i} - \pi_{B2_i} \right)^2 + C \left(+y_1 - y_2 + y_3 - y_4 - \pi_{C1_i} + \pi_{C2_i} \right)^2 \} \quad \text{(A1)}$$

where n is the number of cells. The local elastic modulus is proportional to the basis weight density ρ_i. The quantity α_i denotes the integrity of the cell: $\alpha_i = 1$ for intact cells and $\alpha_i = 0$ for completely failed cells. The prefactors A, B, and C are related to the Young's modulus E and shear modulus G through $A = E/8$, $B = (E+G)/24$, and $C = G/8$, respectively. In the simulations, external strain is increased gradually. The nodal displacements are obtained by minimizing the above elastic energy. Individual cells are usually allowed to yield before failure. This is accomplished by assigning an irreversible displacement component π separately for each of the three deformation modes in Fig. 3. Initially all the πs are zero but, as the external strain increases, the πs start to grow irreversibly according to:

$$\begin{aligned}
\pi_{A_i}^{k} &= \max\left(\pi_{A_i}^{k-1}, \left(y_1 + y_2 - y_3 - y_4 - 2\theta_A \right) \right) \\
\pi_{B1_i}^{k} &= \max\left(\pi_{B1_i}^{k-1}, \left(y_1 - y_3 - \theta_B \right) \right) \\
\pi_{B2_i}^{k} &= \max\left(\pi_{B2_i}^{k-1}, \left(y_2 - y_4 - \theta_B \right) \right) \\
\pi_{C1_i}^{k} &= \max\left(\pi_{C1_i}^{k-1}, \left(y_1 - y_4 - \theta_C \right) \right) \\
\pi_{C2_i}^{k} &= \max\left(\pi_{C2_i}^{k-1}, \left(y_2 - y_3 - \theta_C \right) \right)
\end{aligned} \quad \text{(A2)}$$

The yield thresholds are defined as $\theta_A = \theta_B = \theta_{pl}$ and $\theta_C = [2(1 + \theta_{pl})^2 - 1]^{1/2} - 1 \approx 2\theta_{pl}$, where θ_{pl} is the longitudinal threshold strain of the isotropic material. The value of θ_C arises from the diagonal strain of the cell. Cell failure is defined by another critical strain θ_{fr}. The model describes a brittle elastic material if $\theta_{fr} = \theta_{pl}$.